A new approach for estimating the effective froth height on column trays

Vishwakarma, V.; Wiedemann, P.; Schleicher, E.; Schubert, M.; Hampel, U.;

Originally published:

November 2020

Chemical Engineering Science 231(2021), 116304

DOI: https://doi.org/10.1016/j.ces.2020.116304

Perma-Link to Publication Repository of HZDR:

https://www.hzdr.de/publications/Publ-31491

A new approach for estimating the effective froth height on column trays

Vineet Vishwakarma[a,b,*], Philipp Wiedemann[a], Eckhard Schleicher[a],
Markus Schubert[a,*], and Uwe Hampel[a,b]

[a]Institute of Fluid Dynamics, Helmholtz-Zentrum Dresden-Rossendorf, Bautzner Landstraße 400, 01328 Dresden, Germany

[b]Chair of Imaging Techniques in Energy and Process Engineering, Technische Universität Dresden, 01062 Dresden, Germany

*Corresponding authors: m.schubert@hzdr.de (M. Schubert)
v.vishwakarma@hzdr.de (V. Vishwakarma)

Abstract: The present work proposes a new approach for measuring the effective froth height on column trays. This approach is applied to the two-phase dispersion data gathered by a novel multi-probe sensor installed inside a large-scale tray column mockup. A physical explanation of the proposed approach describes how to distinguish between the liquid-continuous and gas-continuous regions in the froth. Accordingly, the effective froth height distributions are reported at selected tray loadings.

Keywords: effective froth height, column tray, froth-spray transition, conductivity probes.

1. Introduction

Two-phase froth is often encountered in industrial tray columns.[1,2] It comprises of a liquid-continuous region and a gas-continuous region as exemplarily shown in Fig. 1.[3,4] The proportion of each region in the overall froth depends on tray design, system and operating conditions.[5-7] Since these regions have different dispersion characteristics, their hydrodynamic and mass-transfer behavior require individual considerations.[2,5,8-11] Therefore, it is crucial to identify the respective region boundaries, or in other words the individual region heights in the overall dispersion.

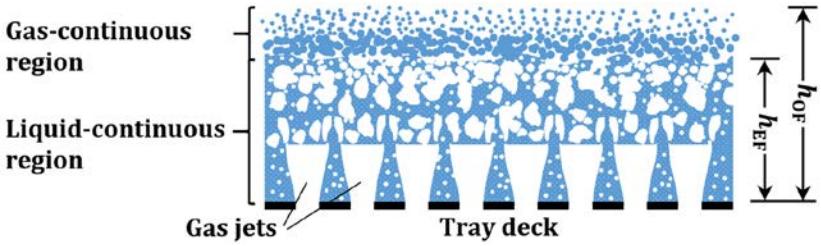

Figure 1. Froth illustration on a sieve tray.

In the literature, the uppermost froth boundary (referred to as the overall froth height (h_{OF}) above the tray deck) in Fig. 1 is discerned either visually or via traversing liquid holdup measurements using γ-ray densitometry.[1,2,6,8,12,13] The densitometry studies used the lowest detectable liquid holdup as a threshold to determine the overall froth height. γ-ray computed tomography is also used in the literature,[14-18] but, mainly for process monitoring and troubleshooting purposes. However, these studies have not detected the transition between the two regions, possibly because of the irregular nature of the complex gas-liquid interface.[8]

The present work proposes a new approach for measuring the height of the liquid-continuous regime above the deck, which is referred to as the effective froth height (h_{EF}) in Fig. 1. The new approach utilizes the data obtained from fast-responding local conductivity probes exposed to the froth on

trays. The approach is illustrated for data obtained with a novel flow profiler,[19-21] which is a multi-probe sensor installed on a large-scale sieve tray. A physical explanation of the proposed approach describes how to distinguish between the liquid-continuous and gas-continuous regions in the froth. The results of the new approach are also compared with those from correlations.

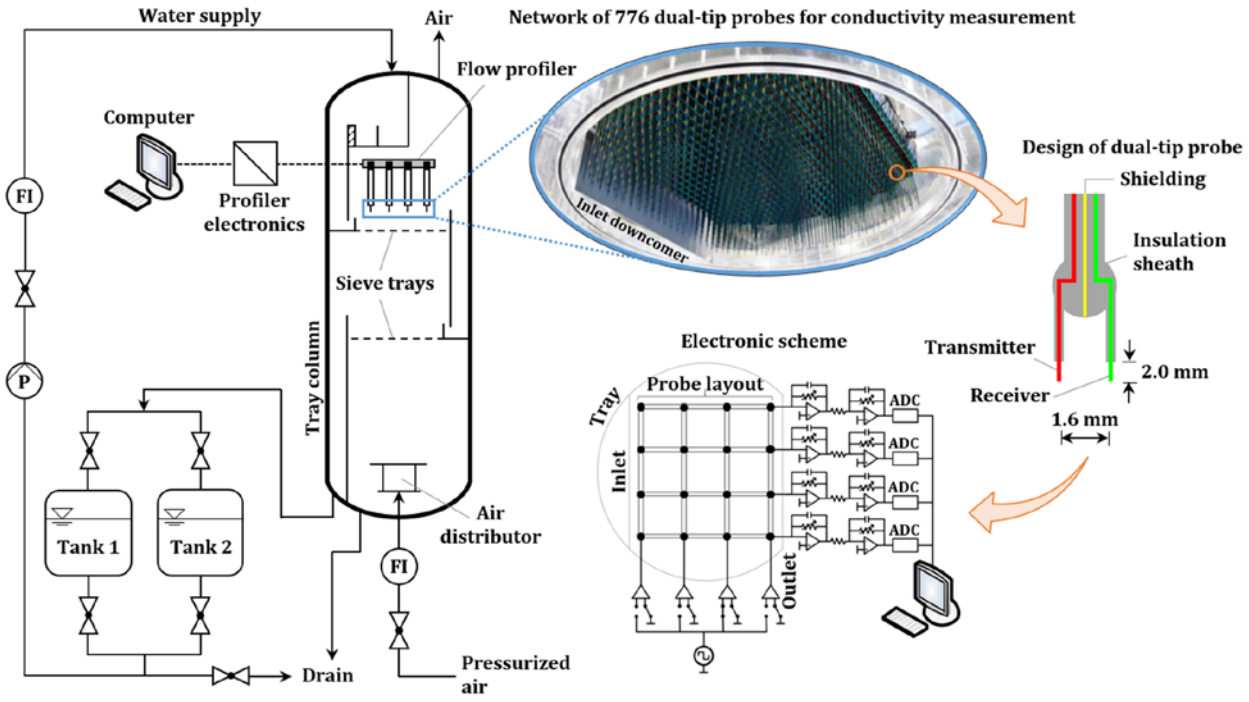

Figure 2. Illustration of column facility and flow profiler (with probe design and electronic scheme exemplarily depicted for a 4 × 4 probe layout).

2. Column mockup and flow profiler

An existing air/water column simulator (of 0.8 m internal diameter) equipped with two sieve trays (each with 13.55% free area) is used in this work. A high-pressure blower supplies air to the column, whereas the water is pumped to the column top (Fig. 2). The gas load on the trays is 1.98 $Pa^{0.5}$, and the liquid loads are 2.15 $m^3/(m^2h)$, 4.30 $m^3/(m^2h)$ and 6.45 $m^3/(m^2h)$. The steady column operation

ensures uniform liquid temperature and conductivity in the column. Further specifications of the tray column are summarized in Table S1 in the Supplementary Information.

Fig. 2 also shows the profiler configuration comprising of 776 dual-tip conductivity probes spanning over the active tray area. The spatial resolution of the profiler is 21 mm × 24 mm, i.e., given by the inter-probe distance. Each probe is a multilayer printed circuit board enclosing three electrodes (i.e. transmitter, receiver and shielding) in an insulating sheath (see Fig. 2). The transmitter and receiver tips only are exposed to the dispersion. A skeletal grid of 28 × 32 headers holds all probes and connects them to the profiler electronics, whose schematics are exemplarily shown for a 4 × 4 grid in Fig. 2. A constant excitation voltage is applied to the transverse headers sequentially via multiplexing scheme, thereby activating the corresponding probe transmitters. Parallel sampling of the longitudinal headers records the electric current acquired by all probe receivers, simultaneously, based on the local instantaneous conductance near the tips. The received signals are amplified, digitized and stored as a 3D data matrix of size $32 \times 28 \times n$, where n equals the total measurement time (= 300 s) times the sampling frequency (= 5000 Hz). This way, the profiler records the two-phase planar data one by one at multiple elevations above the deck via manual adjustments. Further description of the experimental facility and the flow profiler are separately available.[20]

3. New approach for region identification

An estimation of the effective froth height relies on the profiler's ability to distinguish the liquid-continuous and gas-continuous regions along the measurement height. Fig. 3a elucidates the signal responses of an individual probe exposed to the single-phase and two-phase flow of air and water. A zero signal is registered for the probe exposed to air. Contrarily, a droplet covering the probe tips assures a complete transfer of electric current from transmitter to receiver based on the local electri-

cal conductivity. Coincidently, the droplet also ensures a large geometry factor amidst the tips resulting in the highest response signal (= L_2 in Fig. 3a). A high geometry factor also applies for the probes immersed in the liquid. However, a fraction of the transmitted current dissipates to the nearby probes at ground potential (see electronic scheme in Fig. 2) that reduces the response to L_1 in Fig. 3a. Single-phase responses are useful for illustrating the complex two-phase responses.

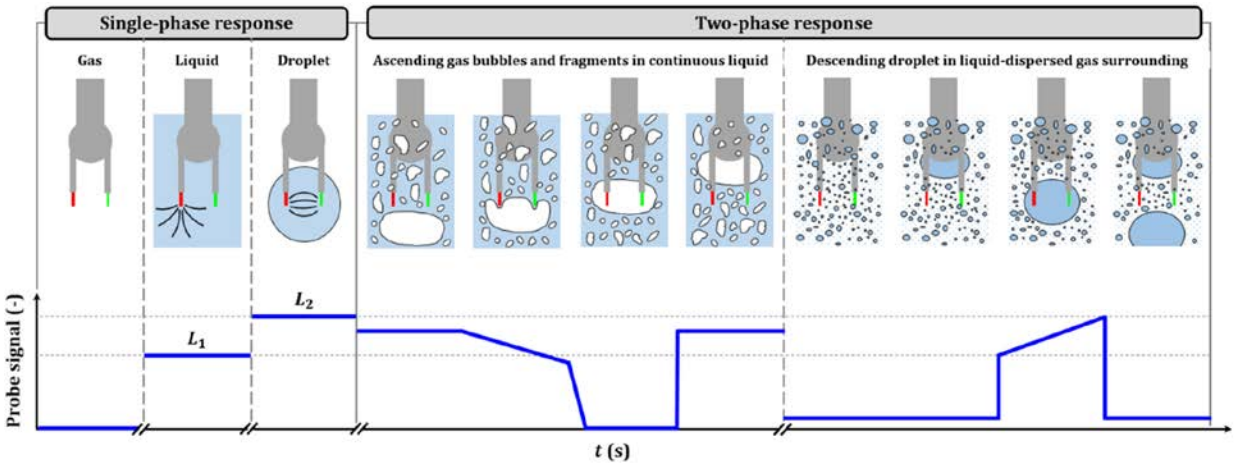

(a)

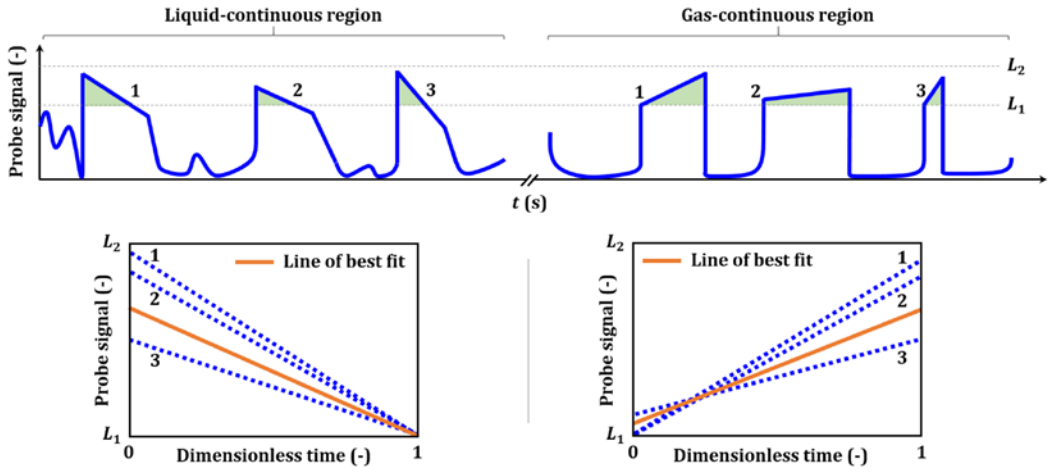

(b)

Figure 3. (a) Schematics of the probe responses to froth dispersion, and (b) characteristic probe time-series signal (upper row) with estimated slopes utilized for the region identification.

In the liquid-continuous region, dispersed gas in the probe vicinity resists the current flow to the nearby probes at ground potential as well as reduces the geometry factor. Here, the probe signal is bounded by L_1 and L_2 as shown in Fig. 3a. Now, when a larger gas volume approaches the probe tips, the surface tension of the liquid inhibits the gas penetration that steadily lowers the signal (negative slope) owing to the decreasing geometry factor. Afterwards, the gas interaction with the probe returns a zero signal, until it encounters the continuous liquid again.

A probe exposed to dispersed liquid in the continuous gas records a signal significantly lower than L_1 as depicted in Fig. 3a. However, the liquid droplets continuously settle on the probe shaft and gravitate while coalescing beneath the joint holding two electrodes (see Fig. 3a and the video in the Supplementary Information). Eventually, the droplet passes the tips facilitating the current flow between them. Before falling off the probe, the droplet growth causes a steady increase in the geometry factor accompanied by a steady rise (positive slope) in the probe signal between L_1 and L_2 as shown in Fig. 3a. Note that the lower limit of the rising signal arbitrarily stated as L_1 can be any value below L_2.

As liquid is continuous until the L_1 response, the new approach proposes retrieving the data above L_1 and arranging them on a dimensionless time-scale. Three such instances (shaded and numbered) are exemplarily shown for each regime in Fig. 3b (not drawn to scale). Then, the retrieved data are fitted with a straight line using the polyfit function in MATLAB®. According to the probe responses above L_1 in Fig. 3a, the 'line of best fit' returns a negative slope in the liquid-continuous region and a positive slope in the gas-continuous region (see Fig. 3b) and acts as a region identifier in this approach. This procedure is repeated at several elevations above the tray deck. Eventually, the local effective froth height is the one, where the slope value approaches zero (Fig. 4). Finally, the mean of the 776 local effective froth heights gives the average effective froth height (h_{EF}) on the tray.

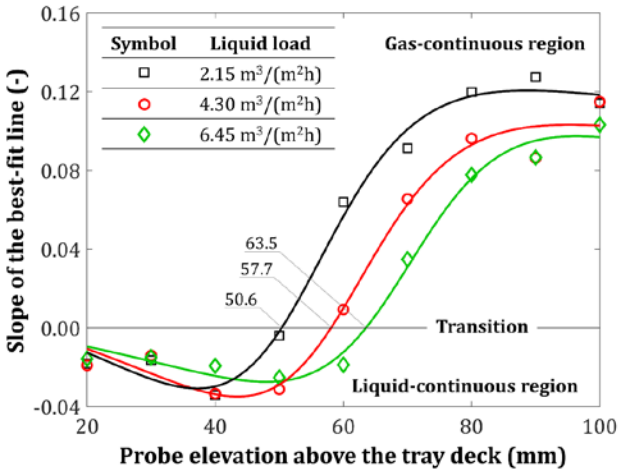

Figure 4. Slope variation with probe elevations and fitted functions for the given loadings.

4. Results and discussion

The profiler records the two-phase dispersion data between 20 mm and 100 mm elevations above the deck in increments of 10 mm. The L_1 response (see Fig. 3) is obtained by immersing the probes in a liquid pool with identical temperature and conductivity as observed during the two-phase experiments. Details on the profiler data acquisition can be found elsewhere.[20] As discussed in Section 3, the slope of the line of best fit is calculated for these elevations. For instance, the slope values at different elevations of the probe [5,13] is shown in Fig. 4 for different loadings. The local effective froth height cannot be derived directly from the discrete slope values. For better illustration, the data points for each load are fitted with a quadratic/quadratic rational function in Fig. 4. The stated functions are nearly linear at the region transition (i.e. between the data points immediately above and below the zero-slope line). Eventually, the local effective froth height is calculated from those points using linear interpolation. The local effective froth heights are 50.6 mm, 57.7 mm and 63.5 mm for the loadings 2.15 $m^3/(m^2h)$, 4.30 $m^3/(m^2h)$ and 6.45 $m^3/(m^2h)$, respectively, in Fig. 4.

Fig. 5 shows the effective froth height distributions on the tray for the specified loadings along with the corresponding averaged heights (h_{EF}). A linear increase in h_{EF} with liquid loading is observed

here. For all loads, the height of the liquid-continuous region is largely uniform over the tray except near the inlet. The inlet-calming zone holds minimum froth heights because of no aeration there. Furthermore, the inlet weir projects the downcomer backup to a certain elevation on the tray. Coincidently, liquid accumulation near the inlet forces the gas from first few holes to interact with the projected liquid leading to a maximum effective froth height in that region. Moreover, to check the data reproducibility, the 300 s time-series signal pertaining to each probe is divided into two datasets of 150 s duration for each loading. The overall procedure described so far computes nearly the same average effective froth heights (as given in Fig. 5), whose evidences are furnished in Table S2 in the Supplementary Information.

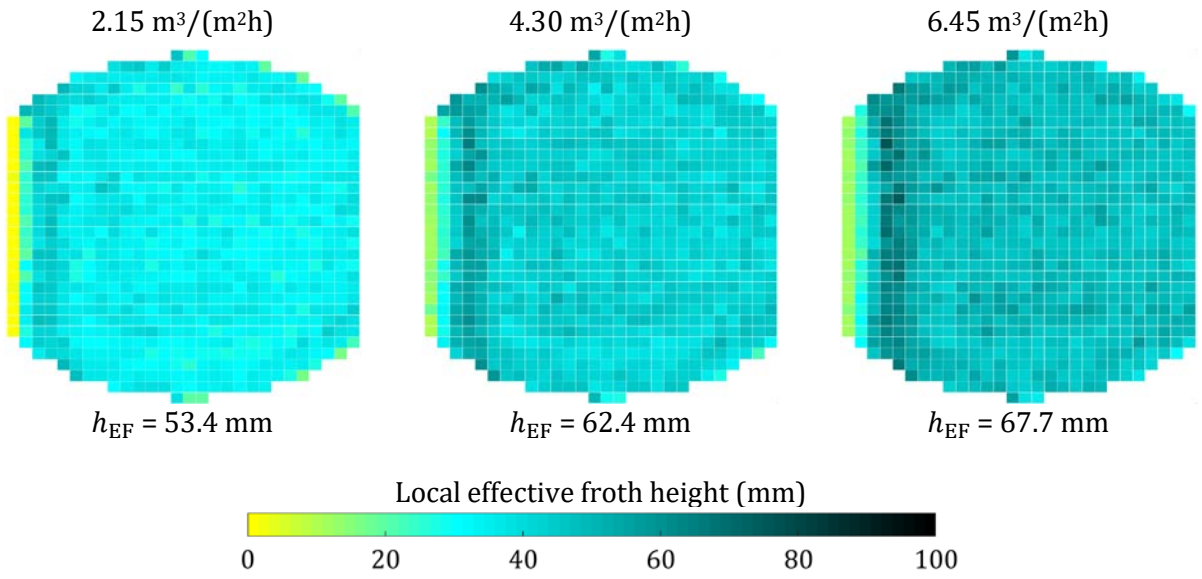

Figure 5. Effective froth height distributions for the given loadings (left edge – inlet, right edge – outlet).

Hitherto, no direct correlation is available for predicting the effective froth height. Bennett et al.[3,4] proposed a correlation for the clear liquid height that includes a model for predicting the average liquid holdup in the liquid-continuous region. The average effective froth height can be predicted

from these parameters, whose details are provided in Section S3 in the Supplementary Information. Although the measured and predicted heights show the same trend for the given loadings (Fig. 6), the correlation underestimates them.

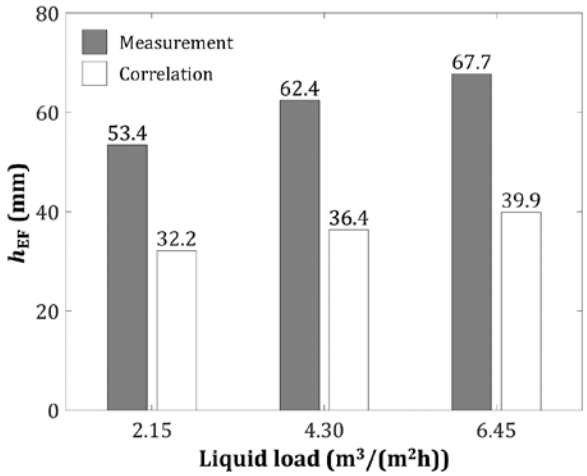

Figure 6. Measurement and prediction of the average effective froth height.

5. Conclusion

A new approach for measuring the effective froth height has been proposed. This approach has been applied to the two-phase dispersion data acquired by multiple dual-tip conductivity probes of a new flow profiler in an air/water sieve tray column mockup. A physical basis of this approach has been elaborated for distinguishing the liquid-continuous and gas-continuous regions in the probe vicinities. This has led to effective froth height distributions at specified tray loadings. Although this approach has been illustrated for conductivity probes, a similar approach is possible for any other tip probe technique that accounts for the local phase fraction in a similar manner, such as optical probes etc.

Funding

This work was supported by the German Federal Ministry for Economic Affairs and Energy (Bundesministerium für Wirtschaft und Energie, BMWi, grant number: 20835 BG/1). V.V. acknowledges the financial support from German Academic Exchange Service (Deutscher Akademischer Austauschdienst, DAAD, grant number: 91563198).

References

1. Lockett MJ, Kirkpatrick RD, Uddin MS. Froth regime point efficiency for gas-film controlled mass transfer on a two-dimensional sieve tray. *Trans Inst Chem Eng.* 1979;57(1):25-34.
2. Lockett MJ. *Distillation tray fundamentals.* Cambridge University Press; 1986.
3. Bennett D, Agrawal R, Cook P. New pressure drop correlation for sieve tray distillation columns. *AlChE J.* 1983;29(3):434-442.
4. Bennett DL, Kao AS, Wong LW. A mechanistic analysis of sieve tray froth height and entrainment. *AlChE J.* 1995;41(9):2067-2082.
5. Val Pinczewski W, Benke ND, Fell CJ. Phase inversion on sieve trays. *AlChE J.* 1975;21(6):1210-1213.
6. Bernard J, Sargent R. The hydrodynamic performance of a sieve plate distillation column. *Trans Instn Chem Engr.* 1966;44:314-327.
7. Békássy-Molnár E, Mustafa H. Clear liquid height on sieve plates in the froth, mixed and spray regimes. *Chem Eng Res Des.* 1991;69(1):14-20.
8. D'Arcy D. *Analysis of sieve tray froths such as occur in heavy water production plants.* Canada1978. AECL-5828.
9. Pinczewski W, Fell C. Nature of the two-phase dispersion on sieve plates operating in the spray regime. *Trans Inst Chem Eng.* 1974;52(3):294-299.
10. Jeronimo MAdS, Sawitowski H. Phase inversion correlation for sieve trays. Vol 51: Trans Inst Chem Eng; 1973:265-266.
11. Garcia JA, Fair JR. A fundamental model for the prediction of distillation sieve tray efficiency. 2. Model development and validation. *Ind Eng Chem Res.* 2000;39(6):1818-1825.
12. Hofhuis PAM. *Flow regimes on sieve-trays for gas/liquid contacting*, Technische Hogeschool Delft; 1980.

13. Raper JA, Kearney M, Burgess J, Fell C. The structure of industrial sieve tray froths. *Chem Eng Sci.* 1982;37(4):501-506.
14. Jaafar A. Gamma ray scanning for troubleshooting, optimization and predictive maintenance of distillation columns. *Hydrocarbon Asia.* 2005:62-65.
15. Haraguchi MI, Calvo WAP, Kim HY. Tomographic 2-D gamma scanning for industrial process troubleshooting. *Flow Meas Instrum.* 2018;62:235-245.
16. Kemoun A, Rados N, Li F, et al. Gas holdup in a trayed cold-flow bubble column. *Chem Eng Sci.* 2001;56(3):1197-1205.
17. Aquino DD, Mallillin JP, Sulit RF, Hila FC, Nuñez IAA, Bulos AD. Performance evaluation of a rectifier column using gamma column scanning. *Nukleonika.* 2017;62(4):285-287.
18. Gorak A, Schoenmakers H. *Distillation: operation and applications.* Academic Press; 2014.
19. Hampel U, Schubert M, Döß A, et al. Recent advances in experimental techniques for flow and mass transfer analyses in thermal separation systems. *Chem Ing Tech.* 2020;92(7):926–948.
20. Vishwakarma V, Schleicher E, Bieberle A, Schubert M, Hampel U. Advanced flow profiler for two-phase flow imaging on distillation trays. Manuscript under review in Chemical Engineering Science.
21. Vishwakarma V, Schleicher E, Schubert M, Tschofen M, Löschau M, Inventors; Helmholtz Zentrum Dresden Rossendorf eV, assignee. Sensor zur Vermessung von Strömungsprofilen in großen Kolonnen und Apparaten. DE patent DE1020181245012020.

Graphical abstract: